Critical behavior of the three-dimensional Heisenberg antiferromagnet $RbMnF_3$

R. Coldea and R. A. Cowley
Oxford Physics, Clarendon Laboratory, Parks Road, Oxford OX1 3PU, United Kingdom

T. G. Perring
Rutherford Appleton Laboratory, ISIS, Chilton, Didcot OX11 0QX, United Kingdom

D. F. McMorrow
Department of Solid State Physics, Risø National Laboratory, DK-4000 Roskilde, Denmark

B. Roessli*
Institut Laue-Langevin, Boîte Postale 156, F-38042 Grenoble Cédex 9, France
(Received 23 October 1997)

The magnetic critical scattering of the near-ideal three-dimensional Heisenberg antiferromagnet (AF) $RbMnF_3$ has been remeasured using neutron scattering. The critical dynamics has been studied in detail in the temperature range $0.77T_N<T<1.11T_N$, where T_N is the Néel temperature. In agreement with previous measurements, at T_N and for wave vectors away from the AF zone center, the scattering has a quasielastic component in addition to the inelastic response predicted by renormalization-group and mode-coupling theories. Both components scale with the dynamic exponent $z=1.43\pm0.04$, in agreement with dynamic scaling. On cooling below T_N the inelastic peaks transform into the transverse spin waves and a crossover has been observed in the dispersion from a power-law relation $\omega_q=Aq^z$ at T_N to a linear behavior $\omega_q=cq$ in the hydrodynamic region below T_N. The quasielastic component evolves below T_N into the longitudinal susceptibility identified in an earlier polarized neutron experiment. The intensity and energy width of the longitudinal scattering decrease on cooling below T_N. Down to the lowest temperatures where the longitudinal susceptibility could be measured the leading term in the scaling behavior of the energy width was $\gamma_q\approx q^{1.58\pm0.03}$ (hydrodynamic theory predicts a q^2 law). Possible explanations for the observed behavior of the longitudinal susceptibility are discussed. [S0163-1829(98)00310-5]

I. INTRODUCTION

There are a surprising number of unresolved problems in the study of the critical behavior of isotropic magnetic systems of which three are the failure to observe the predicted behavior of the longitudinal susceptibility below T_N, the nature of the crossover from hydrodynamic to critical behavior, and the failure of current theories to predict the observed dynamic response at the critical temperature. Both renormalization-group[1] and spin-wave theories[2] predict that the longitudinal static susceptibility $\chi_L(0)$ is divergent at all $T<T_N$ due to spin-wave fluctuations, whereas it is finite in a mean-field theory that neglects the fluctuations. This behavior arises because of the coupling of the divergent transverse modes into the longitudinal susceptibility. For three-dimensional systems it is predicted that $\chi_L(q)\approx 1/q$, whereas the transverse susceptibility diverges as $1/q^2$. The predicted behavior of $\chi_L(q)$ has not yet been directly observed experimentally. Renormalization-group calculations predict that the longitudinal susceptibility is quasielastic[1] and experiments on both isotropic ferromagnets[3,4] and antiferromagnets,[5] as well as weakly anisotropic antiferromagnets such as MnF_2,[6] are consistent with this conjecture, but the difficulty of the experiments did not allow a detailed determination of the scaling properties.

In the case of the three-dimensional (3D) Heisenberg antiferromagnet both renormalization-group[7,8] (RNG) and mode-coupling[9] (MC) theories predict that the dynamic response at T_N has an inelastic component that arises from heavily damped collective excitations. Measurements have shown, however, an additional quasielastic response[10] that is not explained by these theories. Furthermore, the crossover in the long-wavelength excitations from well-defined spin waves with a linear dispersion in the hydrodynamic regime below T_N to the highly damped excitations at T_N that have a power-law dispersion with the dynamic exponent $z=1.5$ (Ref. 1) has not been studied experimentally.

$RbMnF_3$ is probably the closest realisation of an isotropic 3D Heisenberg antiferromagnet (AF) and is a near ideal $d=3$, $n=3$ system on which to study the critical fluctuations. The manganese Mn^{2+} ions have a large spin-only moment of $S=5/2$ that arises from a half-full $3d$ electronic shell. The magnetic moments are arranged on a simple cubic lattice and are antiferromagnetically coupled by a Heisenberg nearest-neighbor interaction that originates from superexchange through the intervening fluorine F^- ions. The spin waves in $RbMnF_3$ are well explained by linear spin-wave theory with an isotropic exchange constant $J=0.29\pm0.03$ meV between nearest neighbors and a second-neighbor constant of less than 0.02 meV.[11] Antiferromagnetic resonance measurements[12,13] give a negligible magnetic anisotropy of only about 6×10^{-6} of the exchange field. The magnetic anisotropy is low because the Mn^{2+} ion has no orbital moment and because of the cubic symmetry of the site. Mag-

netic ordering occurs below the Néel temperature $T_N = 83$ K, and in this phase the spins align antiferromagnetically along the main diagonals of the cubic unit cell, i.e., along the [1,1,1] crystallographic easy directions.[12,13]

The critical properties of the magnetic phase transition in $RbMnF_3$ have been measured by Tucciarone *et al.*[10] and the values obtained for the static exponents β, ν, γ, and η agree well with those obtained theoretically for a $d=3$, $n=3$ system.[14] Measurements of the dynamic response[10] at T_N showed a quasielastic peak in addition to the inelastic spin-wave peak and the Lorentzian energy width of both components scaled as $\omega \approx q^{1.4\pm0.1}$ in agreement with dynamic-scaling theory, which predicts a $q^{1.5}$ behavior for the characteristic frequency at T_N.[14]

Polarized neutron-scattering experiments[5] below T_N, where the spin fluctuations separate into longitudinal and transverse with respect to the direction of the spontaneous staggered magnetization, have shown that the transverse response is inelastic and dominated by spin waves, while the longitudinal scattering is quasielastic. The longitudinal susceptibility was observed to decrease in intensity with decreasing temperature below T_N, but the difficulty of the polarization experiments precluded a detailed study of the scaling behavior.

In this paper we report results of a series of unpolarized neutron-scattering experiments to study the critical spin dynamics in $RbMnF_3$. From high-resolution measurements we find a nonhydrodynamic scaling of the energy width of the longitudinal susceptibility below T_N, which we argue may arise from the effect of spin-wave fluctuations on the longitudinal modes. We observe a crossover in the dispersion of the long-wavelength excitations from a linear behavior below T_N to a power-law relation with the dynamic exponent $z=1.43\pm0.04$ at the critical temperature. We confirm previous results that showed that the dynamic response at T_N has a quasielastic component in addition to the predicted inelastic response and we characterize the wave vector and temperature dependence of both components.

The rest of the paper is organized as follows. In the next section we describe the experiments. Section III presents the measurements and describes the data analysis for the spin dynamics, first at $T \geq T_N$ and then at $T < T_N$. The results are summarized and discussed in Sec. IV.

II. EXPERIMENTAL DETAILS

The sample used in the experiments was a large single crystal (5 cm^3) of $RbMnF_3$. It was mounted on the cold finger of a closed-cycle cryostat, which provided a variable temperature control in the range 8 K to room temperature with a stability of ± 0.01 K (IN14) and ± 0.001 K (TAS7). The sample was aligned with the $[1, \overline{1}, 0]$ axis vertical so as to allow access to the (0.5,0.5,0.5) reciprocal-lattice point, which becomes the antiferromagnetic zone center in the ordered phase. The cubic lattice parameter was $a=4.239$ Å at 8 K.

The neutron-scattering measurements were performed using the three-axis crystal spectrometers TAS7 at the Risø National Laboratory in Denmark and IN14 at the Institut Laue-Langevin, in Grenoble, France. The presample monochromator of the neutron beam was a pyrolytic graphite (PG) (002) crystal and the energy of the scattered beam was analyzed using the (002) reflection from another PG crystal. Both the monochromator and the analyzer were flat to ensure good wave-vector resolution. The spectrometers were operated with a fixed final wave vector k_F between 1.2 and 1.55 $Å^{-1}$ and a cooled beryllium filter was inserted after the sample to eliminate the higher-order contamination in the beam. The collimations used for TAS7 were $7' \times \lambda(Å)$ -60′ -60′-OPEN with $k_F = 1.55$ $Å^{-1}$ giving an in-plane wave-vector resolution measured at the (0.5,0.5,0.5) magnetic Bragg peak at base temperatures of 2.15×10^{-2} $Å^{-1}$ longitudinal and 1.17×10^{-2} $Å^{-1}$ transverse to the scattering wave vector, while the energy resolution for incoherent elastic scattering was 0.25 meV [full width at half maximum (FWHM)]. A narrower resolution was required for the measurements of the longitudinal susceptibility below T_N and the configuration was changed to $7' \times \lambda(Å)$ -30′ -20′-OPEN and $k_F = 1.3$ $Å^{-1}$ giving an energy resolution of 0.09 meV. At IN14 use was made of the higher flux and a tighter collimation was chosen for better resolution $52'/k_I(Å^{-1})$ -40′ -40′ -40′ with $k_F = 1.2$ $Å^{-1}$ and the corresponding widths were 1.03×10^{-2} $Å^{-1}$, 0.73×10^{-2} $Å^{-1}$, and 0.056 meV.

Constant wave-vector scans in both neutron energy loss and gain were made with the wave-vector transfer $\boldsymbol{Q}$ along the [1,1,1] direction and around the antiferromagnetic zone center (0.5,0.5,0.5), in the temperature range 64 K $< T <$ 92 K, where the Néel temperature was around 83 K. The intensities were measured against a monitor counter placed in the incident beam and appropriate corrections to the data were made for the higher-order contamination in the incident beam.[15] The nuclear incoherent elastic scattering and the instrumental background were measured at base temperature and then subtracted from the scans.

III. RESULTS AND ANALYSIS

A. Measurements at $T \geq T_N$

The transition temperature T_N was determined from the temperature dependence of the elastic scattering measured when scanning the wave-vector transfer in reciprocal space through the (0.5,0.5,0.5) magnetic Bragg position. Using the method suggested by Bruce,[16] T_N was located by the maximum in the temperature derivative of the integrated intensity, which gave $T_N = 82.73 \pm 0.02$ K (TAS7) and 82.93 ± 0.05 (IN14). The small shift of 0.2 K between the two values is probably due to a slight difference in the temperature scales of the two thermometers and in the following all temperatures are given relative to the measured T_N.

Constant wave-vector scans at the Néel temperature and for wave vectors $Q=(0.5+q,0.5+q,0.5+q)$ showed an inelastic, broad peak on both the energy loss and the energy gain side, as well as another peak centered at zero-energy transfer. Measurements were taken for q in the range 0.02–0.12 and a representative summary is shown in Fig. 1, where the structure of the scattering line shape is most apparent at large q's where the inelastic and quasielastic components are better separated in energy. As expected for critical scattering, the intensity decreases and the linewidth broadens with increasing wave vector. The observed inelastic plus quasielastic structure of the dynamic response is consistent with pre-

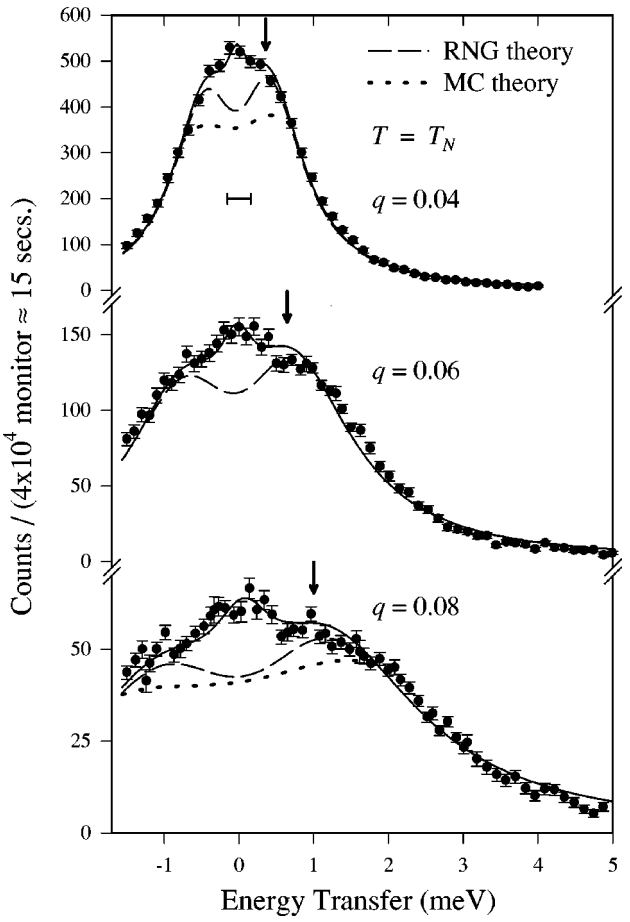

FIG. 1. Critical scattering at T_N as a function of energy and wave vector. Data points have been corrected as described in the text. The asymmetry between the energy loss and energy gain side is well accounted for by the thermal population factor. The solid lines show a fit to Eq. (1) and the long-dashed lines represent the RNG component in the fit, while the arrows above the scans indicate the positions of the inelastic peaks. The prediction of MC theory is shown by the dotted lines in the top and bottom scan for which numerical calculations are available. The spectrometer configuration was TAS7 [7′×λ(Å) -60′-60′-OPEN] with fixed $k_F = 1.55$ Å^{-1} and the measured energy resolution (FWHM) is shown by the horizontal bar in the top scan.

vious measurements[10] and with the results of computer simulations,[17] but disagrees with RNG (Ref. 8) and MC theories,[9] which do not give a peak at zero-energy transfer.

For a quantitative comparison with the two theories, the measurements were fitted to a profile that contained a quasielastic peak of minimum intensity in addition to the predicted line shape. Since both the RNG and the MC scaling functions are constructed to satisfy exact sum rules[9] and to give the correct frequency moments, adding an extra term will violate the sum rules and so this approximation is expected to be valid only if the extra term is relatively small. The choice in the functional form of the quasielastic peak is not unique and a Lorentzian line shape was used since it allowed a good description of the data and also made the comparison easier with measurements below T_N, where a quasielastic peak with a Lorentzian line shape is predicted to arise from longitudinal fluctuations.[1]

The functional form used to analyze the data in terms of RNG theory was

$$I(Q,\omega)=\frac{\omega}{1-e^{-\hbar\omega/k_BT}}\left[\chi_1\frac{f_{RNG}}{\Gamma_1}+\chi_2\frac{\Gamma_2/\pi}{\omega^2+\Gamma_2^2}\right], \quad (1)$$

where the prefactor is due to detailed balance[14] and χ_1 and Γ_1 are the integrated intensity and the characteristic frequency width of the RNG component whose line shape is given by the normalized universal function[7] $f_{RNG}=f(x,\nu)$ defined in the Appendix with $x=\tilde{q}/K$ the reduced wave vector and $\nu=\omega/\Gamma_1$ the reduced frequency; $\tilde{q}=(2\pi/a)\sqrt{3}q$ is the wave vector expressed in units of Å^{-1} and K is the inverse correlation length assumed known from previous measurements[10] $K=0.476[(T-T_N)/T_N]^{0.707}$ (Å^{-1}). The fitting parameters in Eq. (1) are χ_1, Γ_1, the quasielastic peak intensity χ_2, and the Lorentzian half-width Γ_2.

The solid lines in Fig. 1 show the results of the overall fit to Eq. (1), while the long-dashed lines represent the RNG component. Above T_N the inelastic peaks decrease in energy and the scattering line shape progressively transforms into a broad quasielastic peak that can be well described in terms of RNG theory without any extra term as shown in Fig. 2 for $q=0.08$ and $T\geqslant 1.064T_N$. The characteristic energy widths are plotted in Fig. 3, where the solid line labeled Γ_1 is a power-law fit to the scaling behavior at T_N, which gives $\Gamma_1=(82.47\pm 9.3)q^z$ (meV), with $z=1.43\pm 0.04$. A power law with the same exponent can be used to fit the behavior of Γ_2 at T_N with the result $\Gamma_2=(16.9\pm 0.9)q^{1.43}$ (meV) and the fit is shown by the solid line labeled Γ_2 in the figure. The scaling behavior of both components is in good agreement with dynamic scaling theory which gives that the frequency response at T_N increases with wave vector as $q^{1.5}$.[14] The dashed and dotted lines in Fig. 3 show the prediction of RNG theory for the behavior of Γ_1 at two temperatures above T_N and the calculation is in qualitative agreement with the measurements. The curves were plotted using Eq. (A3) in the Appendix

$$\Gamma_1(q)=\Gamma_0(\tilde{q}^{\,2}+K^2)^{z/2}, \quad (2)$$

where Γ_0 and z were determined from the fit to the behavior at T_N, $\tilde{q}$ is the wave vector expressed in Å^{-1}, and K is the inverse correlation length obtained from Ref. 10.

The wave-vector and temperature dependence of the integrated intensities are plotted in Fig. 4(a), χ_1, and Fig. 4(b), χ_2. The solid lines in the figures are power-law fits to the behavior at T_N and give $\chi_1\sim 1/q^{1.73\pm 0.07}$ and $\chi_2\sim 1/q^{1.73\pm 0.2}$, which are close to the $1/q^{2-\eta}$ ($\eta=0.055$) prediction of dynamic scaling theory for the wave-vector dependence of the static susceptibility at T_N.

The fits shown in Figs. 1 and 2 were made without any account of the instrumental resolution. In order to test the effects of the resolution the data was fitted to Eq. (1) convolved with the Gaussian resolution function along the energy axis. For the areas χ_1 and χ_2 fixed the fits gave Γ_1 unchanged to within 1% and Γ_2 smaller by 15% at low q's and by 3% at large q's. The scaling behavior of both widths was similar to the one obtained without resolution deconvolution and so these fits will not be discussed further.

To summarize, it was found that RNG theory gives a good description of the behavior in the hydrodynamic regime above T_N where $\tilde{q}\ll K$. However, in the critical region where

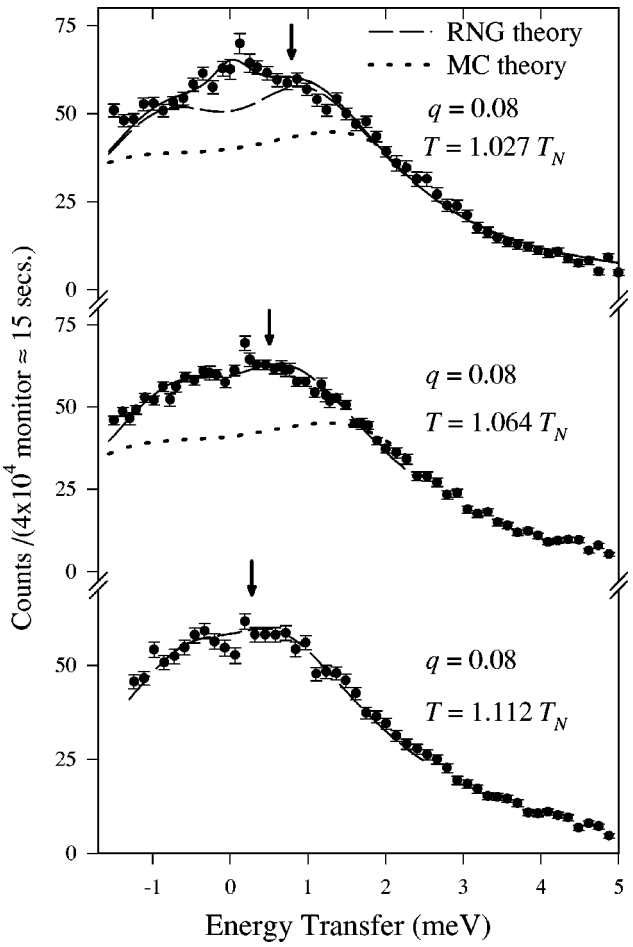

FIG. 2. Critical scattering at $q=0.08$ as a function of energy and temperature. Data points have been corrected as described in the text. At temperatures well above T_N the scattering line shape can be described in terms of RNG theory (dashed line), whereas close to T_N an extra quasielastic peak needs to be included in the fit. The prediction of MC theory is indicated by the dotted lines in the vicinity of the quasielastic position in the top and middle scan for which numerical results are available. The spectrometer configuration was the same as for Fig. 1.

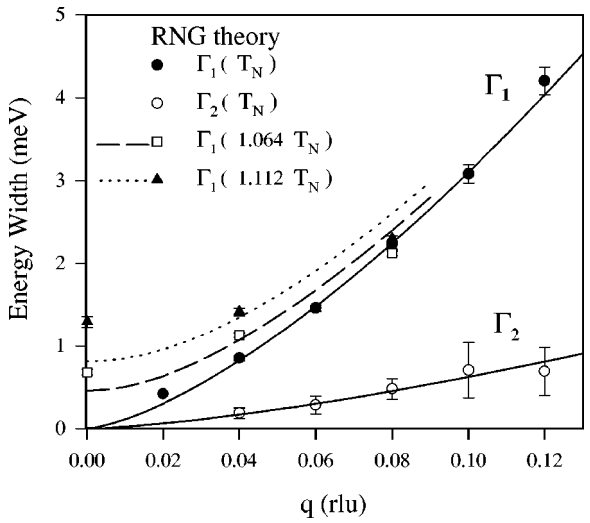

FIG. 3. Wave-vector and temperature dependence of the characteristic energy widths Γ_1 and Γ_2 as extracted from the fit to the RNG theory and a quasielastic peak [Eq. (1)]. The solid lines are power-law fits to the scaling behavior at T_N as described in the text and both have the same exponent $z=1.43$. If not shown error bars are smaller than the size of the points. The dashed and dotted line indicate the calculated behavior of Γ_1 above T_N according to RNG theory [Eq. (2)].

$\tilde{q} \gg K$, the theory predicts the correct value for the dynamic exponent z, but does not explain the quasielastic peak observed in the scaling function.

The mode-coupling theory gives the dynamical response in terms of a system of coupled integral equations.[9] The spectral line shape $f_{MC}(q,\omega)$ at T_N and a selection of temperatures above T_N was calculated numerically by Cuccoli[18] using a wave-vector mesh that spanned the Brillouin zone and had a finest spacing of $\frac{1}{24}(2\pi/a)$, such that results were obtained for the behavior at wave vectors close to the measured points at $q=0$, 0.04, 0.08, and 0.12. The measured line shape was compared with the calculation using a functional form similar to Eq. (1),

$$I(Q,\omega)=\frac{\omega}{1-e^{-\hbar\omega/k_BT}}\left[\chi_1 f_{MC}(q,\omega)+\chi_2\frac{\Gamma_2/\pi}{\omega^2+\Gamma_2^2}\right], \quad (3)$$

where $f_{MC}(q,\omega)$ is the normalized MC spectral line shape and χ_1 is the integrated intensity, while all the other parameters are the same as in Eq. (1). The frequency scale of the theoretical response is already incorporated in the calculated form of the spectral line shape and is not a free parameter in the fit, unlike in the RNG theory [Eq. (1)]. Overall fits to Eq. (3) with the imposed condition that χ_2 is a minimum gave similar results to the solid lines shown in Figs. 1 and 2, where the MC component is indicated by the dotted lines for the wave vectors and temperatures for which numerical calculations are available. The results show that the theory overestimates the linewidth of the dynamic response and consequently a large part of the spectral weight of the observed response at low energies is attributed to the extra quasielastic peak. The wave vector and temperature dependence of the integrated intensities χ_1 and χ_2 were extracted from the fit to Eq. (3) and are shown in Fig. 5, where the solid line is a fit to a power-law relation for the data at T_N giving $\chi_1 \sim /q^{1.84\pm0.08}$ and the dashed lines are guides to the eye. The relative intensity of the quasielastic peak decreases with increasing temperature and with approaching the hydrodynamic regime. The results show that mode-coupling theory, like RNG theory, does not explain the quasielastic peak observed in the dynamic response in the critical region where $\tilde{q} > K$.

B. Measurements at $T<T_N$

In the absence of magnetic anisotropy the magnetic ordering below T_N gives a random arrangement of antiferromagnetic domains. For $RbMnF_3$ the symmetry is not spherical but cubic and there are four equivalent magnetic easy axes along the [111] directions, so that the ordering below T_N consists of four equally populated domains polarized along the easy axes. The scattering from this type of structure is proportional to $\frac{2}{3}[2\chi_T(q,\omega)+\chi_L(q,\omega)]$, so that both transverse and longitudinal susceptibilities are observed.

Constant wave-vector scans at temperatures below T_N and away from the AF zone center showed a well-resolved in-

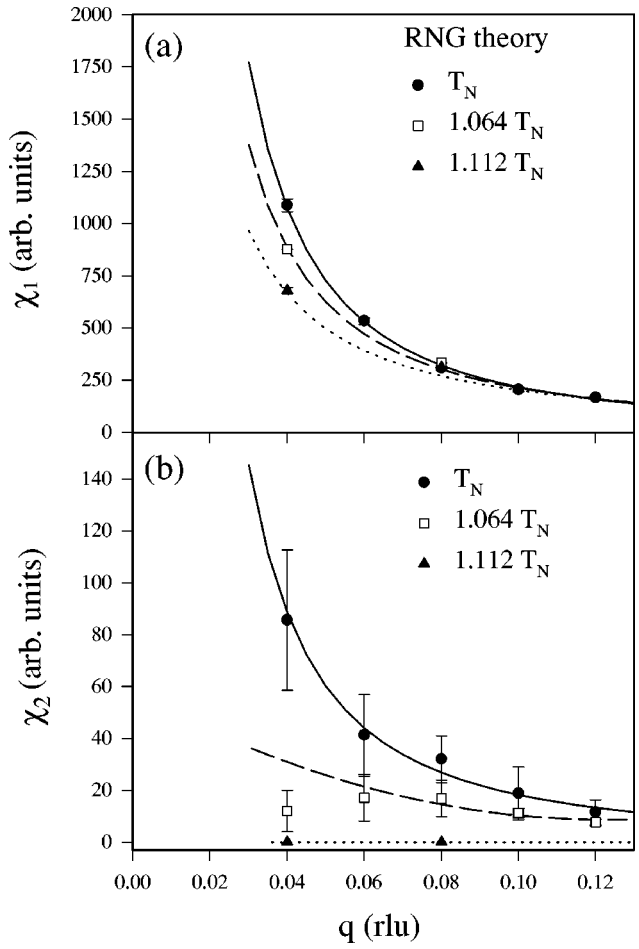

FIG. 4. Wave-vector and temperature dependence of the integrated intensities (a) χ_1 and (b) χ_2 as extracted from the fit to the RNG theory and a quasielastic peak [Eq. (1)]. The solid lines show a fit to a power-law relation as described in the text, while the dashed lines are guides to the eye.

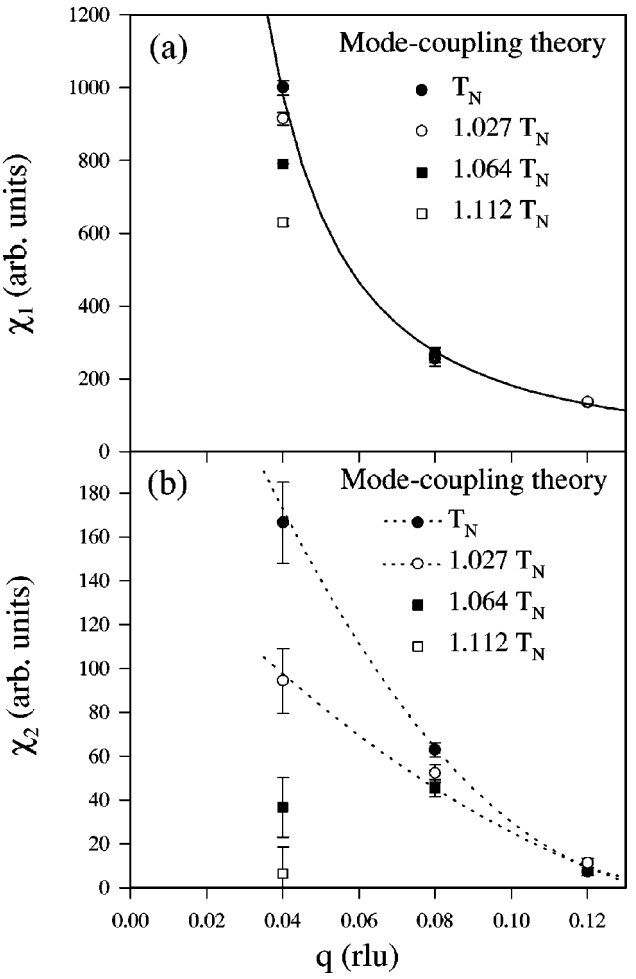

FIG. 5. Wave-vector and temperature dependence of the integrated intensities (a) χ_1 and (b) χ_2 as extracted from the fit to the MC theory and a quasielastic peak [Eq. (3)]. The intensities are expressed in the same units as in Fig. 4. The solid line shows a fit to a power-law relation as described in the text, while the dashed lines are guides to the eye.

elastic excitation together with a small and relatively narrow component centered on zero frequency as shown in Fig. 6 for $q=0.04$. The polarizations of the inelastic and the quasielastic components of the dynamic response below T_N have been studied by earlier polarized neutron-scattering experiments[5] that identified the inelastic peak with the transverse spin waves and the quasielastic peak with the longitudinal scattering.

As the temperature is increased towards T_N the spin-wave peaks decrease in energy, while their linewidth broadens and the overall inelastic intensity increases. The spin-wave line shape was analyzed using a Lorentzian spectrum

$$I(Q,\omega)=\chi_T(q)\frac{1}{2\pi}\left[\frac{\Gamma_q}{(\omega-\omega_q)^2+\Gamma_q^2}+\frac{\Gamma_q}{(\omega+\omega_q)^2+\Gamma_q^2}\right]\frac{\omega}{1-e^{-\hbar\omega/k_BT}}, \quad (4)$$

which was convolved with the four-dimensional Gaussian resolution function of the spectrometer, which was calculated using the Cooper-Nathans formalism.[19] In Eq. (4) ω_q and Γ_q are the spin-wave energy and linewidth and $\chi_T(q)$ is the integrated intensity that gives the wave-vector-dependent transverse static susceptibility. The spin-wave dispersion and the integrated intensity were parametrized with their predicted dependences[1] in the hydrodynamic region below T_N, $\omega_q=cq$, and $\chi_T(q)=B/q^2$, in order to ensure that the correct intensity distribution is taken into account in the convolution, which was performed numerically using a Monte Carlo integration technique. A parametrization of the wave-vector dependence of Γ_q was found to have very little effect on the fitting parameters and consequently Γ_q was assumed to be a constant parameter in the fit. A good description of the data was obtained and a typical fit (which also includes a quasielastic peak to be described below) is shown by the solid line in Fig. 6. The spin-wave energy and integrated intensity were calculated from the fitted values of c and B.

At relatively low temperatures below T_N the dispersion is linear $\omega_q=cq$ and the velocity decreases with increasing temperature, in agreement with the predictions of hydrodynamic theory[1] for wave vectors and temperatures that satisfy $\tilde{q}\ll K$, where K is the inverse correlation length. The dispersion relation at T_N is determined from the positions of the inelastic peaks in the dynamical response when analyzed in

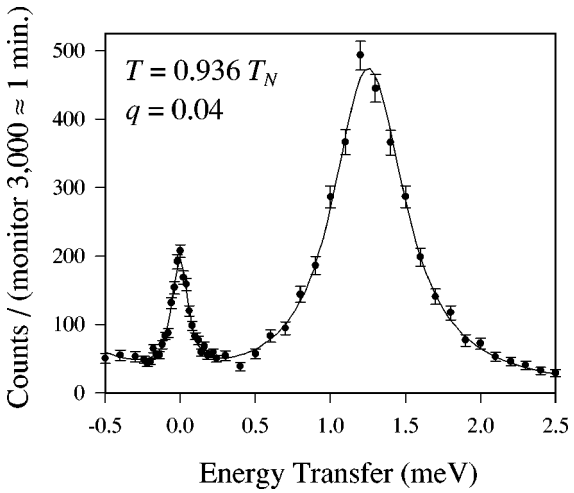

FIG. 6. Constant wave-vector scan at $q=0.04$ and $T=0.936T_N$. Data points have been corrected as described in the text. The solid line is a fit to a Lorentzian spectrum for both the inelastic spin-wave peak and the quasielastic longitudinal scattering, convolved with the instrumental resolution function. The spectrometer configuration was IN14 [52′/k_I (Å^{-1}) -40′ -40′ -40′] with fixed $k_F=1.2$ Å^{-1}.

terms of RNG theory and a quasielastic peak (Fig. 1). The values of the characteristic RNG width Γ_1 are transformed into absolute frequencies of the inelastic peaks using Eq. (A4) and the results give a power-law dispersion relation $\omega_q=Aq^z$, with the exponent $z=1.43\pm0.04$ and $A=37.11\pm4.2$ meV. A gradual crossover from the hydrodynamic to the critical behavior was observed as the temperature approached T_N from below and is presented in Fig. 7. In the intermediate-temperature region a good but not unique fit to the dispersion is obtained by a power-law relation with an exponent that increases from 1 to z as T_N is approached from below and the fits are shown as solid lines in Fig. 7.

The width of the spin-wave peaks scales with wave vector as $\Gamma_q=Dq^{1.41\pm0.05}$ $(0.77T_N\leqslant T<T_N)$ and D increases with

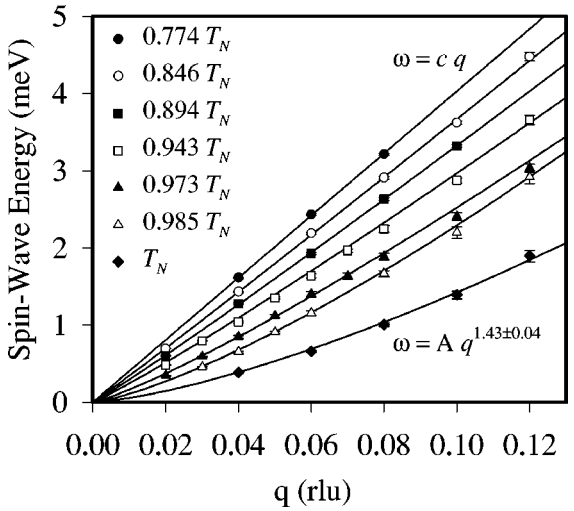

FIG. 7. Spin-wave dispersion as a function of temperature. The solid lines are fits to a power-law relation with an exponent that increases from 1 to z as T_N is approached from below. The dispersion at T_N has been extracted from the positions of the inelastic peaks in Fig. 1.

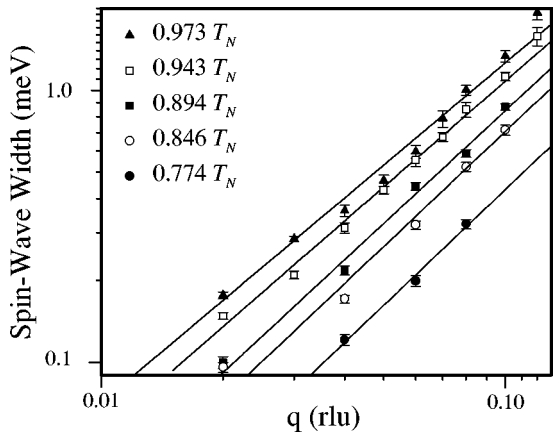

FIG. 8. A log-log plot of the Lorentzian half-width of the spin-wave peaks as a function of wave vector at different temperatures. The solid lines are fits to a power-law behavior.

increasing temperature, as shown in Fig. 8. This behavior is in agreement with dynamic scaling theory, which predicts a $q^{1.5}$ scaling for the characteristic frequency response in the critical region. Hydrodynamic theory predicts $\Gamma_q\approx q^2$ (Ref. 1) and previous measurements[20] at much lower temperatures $(T<0.6T_N)$ observed $\Gamma_q\approx q^{2.13\pm0.18}$.

The integrated intensities are nearly temperature independent for $0.77T_N\leqslant T<T_N$ and are given by $\chi_T(q)=C/q^{1.91\pm0.05}$, as shown in Fig. 9. This result is in good agreement with RNG calculations,[1] which predict a transverse static susceptibility of the form $\chi_T(q)=C/q^2$ with C independent of temperature.

The spin-wave scattering was also analyzed in terms of a damped harmonic oscillator (DHO) line shape[21]

$$I(Q,\omega)=\frac{1}{1-e^{-\hbar\omega/k_BT}}Z_q\frac{\omega\Gamma_q}{(\omega^2-\Omega_q^2)^2+4\omega^2\Gamma_q^2}, \quad (5)$$

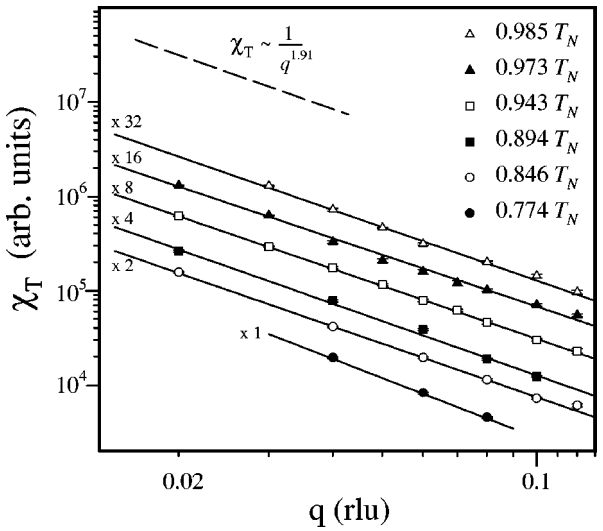

FIG. 9. A log-log plot of the integrated intensity of the spin-wave peaks as a function of wave vector at different temperatures. The error bars are smaller than the size of the symbols. The solid lines are fits to a power law and the dashed line shows the average scaling behavior. For easier comparison successive data sets have been shifted along the vertical axis by multiplication with the factors shown on the left.

where Ω_q is the renormalized spin-wave frequency, Γ_q is the energy width, and Z_q is the one-magnon cross section. Measurements can be well described by Eq. (5) convolved with the instrumental resolution, except for the high-energy tail of the spin-wave peaks at small q's where the DHO line shape gives a faster decrease of the intensity than actually observed. The values obtained for the spin-wave energy Ω_q are larger than the corresponding values of ω_q determined previously, but the scaling behavior is similar: The dispersion is linear at low temperatures and crosses over with increasing temperature to a power-law relation q^z at T_N. The results for Γ_q and for the integrated intensity are also consistent with the behavior obtained when analyzing the line shape in terms of the double Lorentzian spectrum (4) and will not be discussed further.

Based on earlier polarized neutron-scattering experiments,[5] the quasielastic peak observed below T_N was identified with scattering from the longitudinal susceptibility. The longitudinal character is consistent with the observed decrease in intensity on cooling because longitudinal fluctuations are progressively quenched as the ordered moment approaches saturation. The quasielastic peak is considerably broader than the resolution width in the vicinity of T_N, as shown in Fig. 1, and becomes narrower on cooling. Figure 10 presents the wave-vector dependence measured at $0.936T_N$; the linewidth increases and the intensity decreases with increasing wave vector. The quasielastic scattering was analyzed in terms of the predicted Lorentzian line shape for the longitudinal susceptibility[1]

$$I(Q,\omega)=\chi_L(q)\frac{1}{\pi}\frac{\gamma_q}{\omega^2+\gamma_q^2}\frac{\omega}{1-e^{-\hbar\omega/k_BT}}, \tag{6}$$

which was convolved with the four-dimensional Gaussian resolution function of the spectrometer; the results were particularly sensitive to the convolution along the energy axis because the energy width at small q's is comparable to the instrumental resolution indicated by the horizontal bar in the bottom scan of Fig. 10. The integrated intensity $\chi_L(q)$ is identified with the wave-vector-dependent static longitudinal susceptibility and was parametrized in the fit with the predicted behavior[1] $\chi_L(q)=D/q$ to ensure self-consistency of the intensity distribution during the convolution with the resolution function. The spin-wave scattering was also included in the fit in order to account for the curved background under the quasielastic peak that arises from the superposition of the low-energy tails of the spin-wave peaks on the energy-loss and -gain sides. Good fits to the data were obtained and are shown as solid lines in Fig. 10. The wave-vector dependence of the energy width was fitted to a power-law relation with the result $\gamma_q=(8.08\pm0.8)q^{1.58\pm0.03}$ (meV) at $T=0.936T_N$. A power law with the same exponent can be used to fit the data at higher temperatures up to T_N and results are summarized in Fig. 11(a). A fit to the predicted hydrodynamic q^2 dependence including higher-order corrections $\gamma_q=Aq^2+Bq^4$ is shown by the solid line in Fig. 11(b) and is obtained for $A=34\pm2$ meV and $B=-1930\pm550$ meV ($T=0.936T_N$), which give a correction term that is 36% of the leading term at $q=0.08$.

The integrated intensity $\chi_L(q)$ was extracted from the fitted value of the parameter D and the wave-vector and temperature dependence is shown in Fig. 12(a). The longitudinal static susceptibility $\chi_L(q)$ increases with increasing temperature towards T_N and with decreasing wave vector, but the exact analytical form is difficult to extract since the data close to $q=0$ is limited. The results are consistent with the predicted $1/q$ behavior [fits are shown as dashed lines in Fig. 12(a)], given that this divergent behavior is expected to hold only in the region of low q's ($\tilde{q}\ll K$), which becomes smaller on approaching T_N from below.

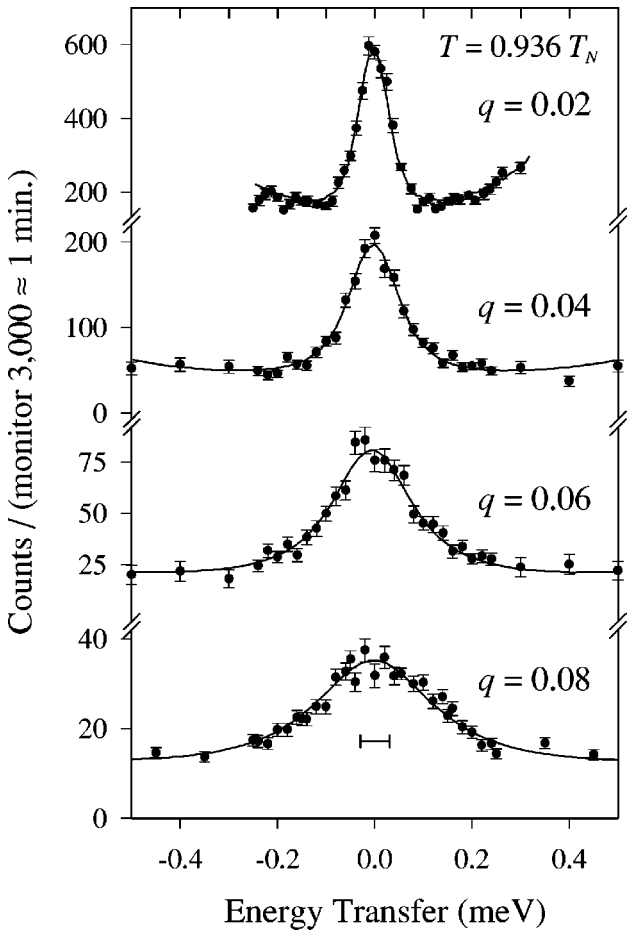

FIG. 10. Longitudinal scattering as a function of energy and wave vector at $T=0.936T_N$. Data points have been corrected as described in the text. The solid lines are fits to a Lorentzian line shape convolved with the resolution function. The horizontal bar in the bottom scan represents the measured energy resolution (FWHM). The background under the quasielastic peaks comes from the low-energy tail of the spin waves on either side. The spectrometer configuration was the same as for Fig. 6.

The values of γ_q and $\chi_L(q)$ are practically unchanged if the static susceptibility is alternatively parametrized using the mean-field formula

$$\chi_L(q)=\chi_L(0)\frac{K_L^2}{q^2+K_L^2}, \tag{7}$$

where $\chi_L(0)$ is the bulk susceptibility, K_L is the inverse correlation length, and the fit to Eq. (6) is performed self-consistently. Figure 12(b) shows the wave-vector and temperature dependence of χ_L and the dashed lines are fits to Eq. (7). The amplitude $\chi_L(0)$ and the correlation length K_L^{-1}

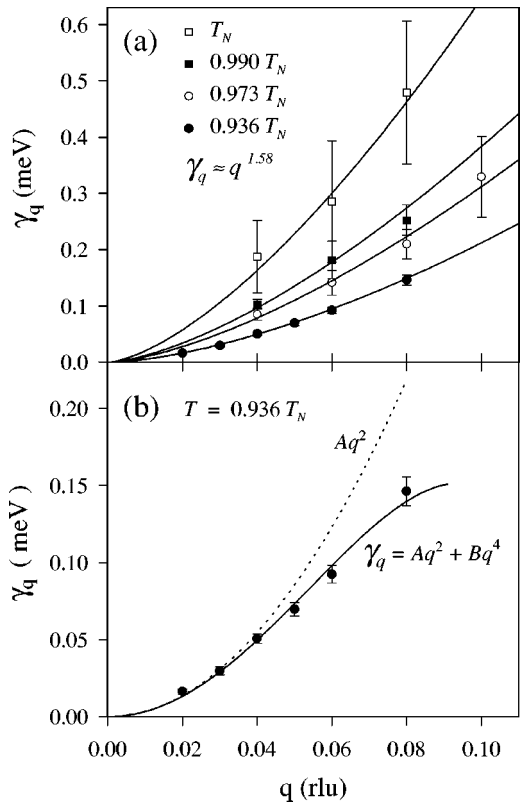

FIG. 11. (a) Lorentzian half-width γ_q of the quasielastic scattering as a function of wave vector and temperature. The solid lines are fits to a power-law relation with the same exponent $q^{1.58}$. (b) Width γ_q at $T=0.936T_N$ fitted to the predicted hydrodynamic behavior plus a correction term Aq^2+Bq^4 (solid line), where the dashed line shows the Aq^2 component in the fit.

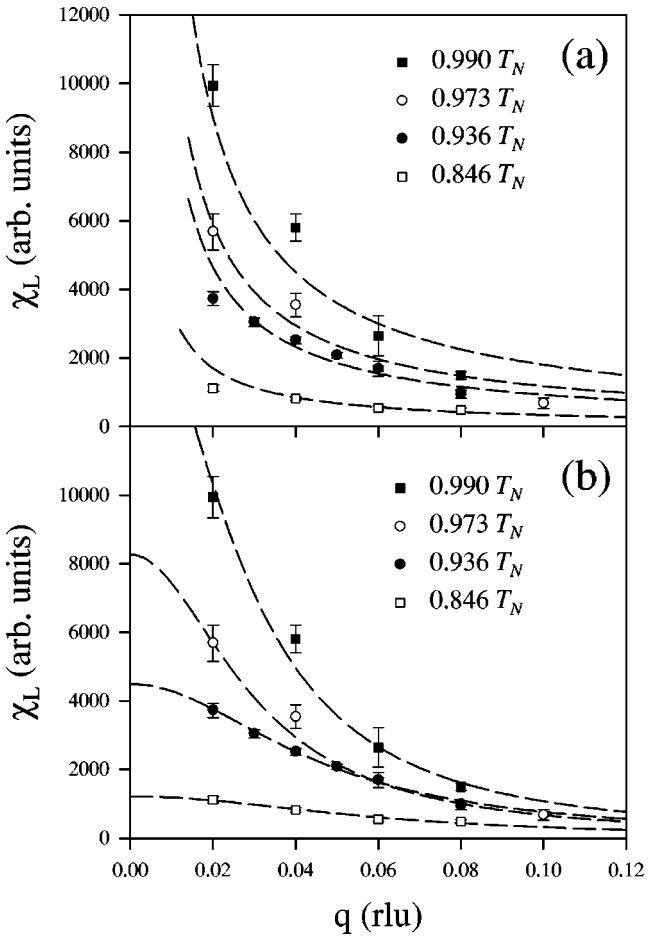

FIG. 12. Integrated intensity of the quasielastic scattering as a function of wave vector and temperature. The dashed lines are fits to (a) the $1/q$ behavior and (b) the mean-field formula (7).

increase as expected on approaching T_N from below, but the values for K_L are a factor of 3–4 larger than those estimated from measurements of the inverse correlation length above T_N (Ref. 10) and from the calculated universal ratios of critical amplitudes below and above the critical point.[22]

IV. DISCUSSION AND CONCLUSIONS

The results summarized in Fig. 1 clearly show that the dynamic response at T_N has a quasielastic as well as an inelastic component. The inelastic response is the signature of collective excitations that are highly damped due to the critical fluctuations, whereas the quasielastic peak is probably due to a relaxational spin diffusion process. The behavior of both the total intensity and of the linewidth of the critical scattering is in agreement with the general predictions of dynamic scaling theory. However, the detailed form of the scaling function disagrees with the predictions of both renormalization-group[8] and mode-coupling theories,[9] which do not explain the quasielastic peak. From continuity arguments with the results obtained below T_N we suggest that the diagrams that contribute to the longitudinal susceptibility and give rise to a quasielastic peak below T_N should also be included in the renormalization-group calculation in the critical region around T_N. Figure 2 shows that with increasing temperature and on approaching the hydrodynamic regime above T_N the scattering line shape transforms into a single quasielastic peak and RNG theory becomes an adequate description, whereas MC theory still slightly overestimates the linewidth.

Below T_N there are both transverse excitations or spin waves with an inelastic spectrum and longitudinal fluctuations, which have relaxational, quasielastic dynamics. The spin waves evolve on cooling from the highly damped collective excitations observed at T_N and, as shown in Fig. 7, the dispersion changes from a power law q^z ($z=1.43 \pm 0.04$) at T_N to a linear behavior appropriate for antiferromagnetic spin waves in the hydrodynamic limit below T_N. At present there is not a unified theoretical description of this crossover between the critical and hydrodynamic regime, although renormalization-group theory provides a good description of the excitations in the two limiting cases.[1]

The quasielastic component of the dynamic response at T_N transforms into the longitudinal scattering on cooling below T_N. Both the intensity and the energy width of this quasielastic response decrease on cooling as predicted by renormalization-group calculations.[1] Down to the lowest temperatures where the longitudinal susceptibility could be measured ($0.936T_N$) the leading term in the scaling of the energy width was found to be $q^{1.58\pm0.03}$ ($0.936T_N<T<T_N$) and no evidence for a crossover to the q^2 behavior predicted by hydrodynamic theory was observed. This result suggests that the theory of the longitudinal susceptibility needs extending because the hydrodynamic treatment neglects the ef-

fect of spin-wave fluctuations on the longitudinal modes. It has been shown theoretically[1] and confirmed experimentally[23] that this coupling leads to a nonhydrodynamic scaling behavior of the energy width of the longitudinal susceptibility for wave vectors close to the ferromagnetic zone center. Our experiments are performed at the antiferromagnetic zone center and also show a nonhydrodynamic scaling behavior.

Resolution considerations put a lower limit on the smallest wave vector q for which the longitudinal susceptibility could be measured reliably in our experiments and as a consequence did not allow a conclusive test of the predicted divergence of the static susceptibility $\chi_L(q)$ at low q's. However, the results shown in Fig. 12(a) are consistent with the predicted $1/q$ behavior; the description in terms of the mean-field theory shown in Fig. 12(b) is difficult to interpret since the resulting values for the inverse correlation length K_L are much larger than expected from measurements above T_N.

ACKNOWLEDGMENTS

We acknowledge financial support for the experiments from the EPSRC in Grenoble and Oxford, and the EU TMR program in Risø. We would like to thank Professor S. W. Lovesey for stimulating our interest in this problem and we appreciate useful discussions with him and with Professor V. Tognetti. We extend thanks to Dr. A. Cuccoli for providing the results of the mode-coupling calculations and also to Dr. D. A. Tennant for help with calculating the resolution convolution. R.C. is grateful to the University of Oxford for financial support.

APPENDIX: SCALING FUNCTION AT $T \geqslant T_N$

The wave-vector and frequency-dependent correlation function of a spin system can be expressed using the dynamic scaling form as[24]

$$C(q,\omega)=\chi(q)\frac{f(x,\nu)}{\Gamma(q,K)}, \tag{A1}$$

where $\chi(q)$ is the static susceptibility, $\Gamma(q,K)$ is the characteristic frequency, $f(x,\nu)$ is the scaling function with the reduced wave vector $x=q/K$ (K is the inverse correlation length), and the reduced frequency $\nu=\omega/\Gamma(q,K)$. Using a RNG approach, Freedman and Mazenko[7] have calculated the scaling function for an isotropic antiferromagnet in $4-\epsilon$ with the result

$$f(x,\nu)=\frac{2}{\mathcal{A}\nu}\mathrm{Im}\frac{\gamma(x,\nu)}{-i\nu+\gamma(x,\nu)}, \tag{A2}$$

where $\mathcal{A}$ is a normalization constant and $\gamma(x,\nu)$ is computed using the relations

$$\gamma(x,\nu)=(\tfrac{1}{3}-i\nu)^{-\epsilon}(\tfrac{1}{4}-i\nu)^{3\epsilon/4}W(x,\nu),$$

$$W(x,\nu)=1+\frac{2\epsilon}{x^2}\Bigg[-t\Delta\ln\sigma+(t-\tfrac{1}{2}b)\ln(1+t-\tfrac{1}{4}b)+\frac{x^2}{4}\ln\left(\frac{\overline{t^2}}{\tau}\right)-\frac{x^2}{8}\ln\tau\Bigg],$$

$$t=-\tfrac{1}{4}(1-x^2)-\tfrac{3}{4}i\nu(1+x^2),$$

$$b=x^2/4,$$

$$\overline{t}=(1+x^2)(1-3i\nu)/4,$$

$$\tau=\tfrac{3}{16}(1+x^2)(1-4i\nu),$$

$$\Delta=(1+b/t^2)^{1/2},$$

and

$$\sigma=\frac{2t(1+t)(1+\Delta)+b}{2t(1+\Delta)-b}.$$

The characteristic frequency has the wave-vector dependence

$$\Gamma(q,K)=\Gamma_0 q^z(1+x^{-2})^{1-\epsilon/4}, \tag{A3}$$

where the dynamic exponent is $z=2-\epsilon/2$. In three dimensions $\epsilon=1$ and the scaling function $f(x,\nu)$ is a Lorentzian centered at $\nu=0$ in the hydrodynamic limit ($x\ll 1$) and it has fluctuation-induced peaks at finite reduced frequency $\nu=\pm 0.45$ in the highly critical region ($x\gg 1$). At T_N these inelastic peaks have the power-law dispersion relation

$$\omega_q=0.45\Gamma(q,0)=0.45\Gamma_0 q^{1.5}. \tag{A4}$$

If $\mathcal{A}=6.2$ in Eq. (A2) the scaling function is normalized to unit area $\int_{-\infty}^{+\infty}f(x,\nu)d\nu=1$ for any value of x, such that the frequency-integrated correlation function gives the wave-vector-dependent static susceptibility $\chi(q)=\int_{-\infty}^{+\infty}C(q,\omega)d\omega$.

*Present address: Laboratory for Neutron Scattering, ETH Zürich and Paul Scherrer Institute, CH-5232 Villigen PSI, Switzerland.

[1] G. F. Mazenko, M. J. Nolan, and R. Freedman, Phys. Rev. B **18**, 2281 (1978).

[2] E. Brézin and D. J. Wallace, Phys. Rev. B **7**, 1967 (1973); E. Brézin, D. J. Wallace, and K. G. Wilson, *ibid.* **7**, 232 (1973); G. F. Mazenko, *ibid.* **14**, 3933 (1976).

[3] P. W. Mitchell, R. A. Cowley, and R. Pynn, J. Phys. C **17**, L875 (1984).

[4] P. Böni, J. L. Martínez, and J. M. Tranquada, Phys. Rev. B **43**, 575 (1991).

[5] U. J. Cox, R. A. Cowley, S. Bates, and L. D. Cussen, J. Phys.: Condens. Matter **1**, 3031 (1989).

[6] M. P. Schulhof, R. Nathans, P. Heller, and A. Linz, Phys. Rev. B **4**, 2254 (1971).

[7] R. Freedman and G. F. Mazenko, Phys. Rev. Lett. **34**, 1575 (1975).

[8] R. Freedman and G. F. Mazenko, Phys. Rev. B **13**, 4967 (1976).

[9] A. Cuccoli, S. W. Lovesey, and V. Tognetti, J. Phys.: Condens. Matter **6**, 7553 (1994).

[10] A. Tucciarone, H. Y. Lau, L. M. Corliss, A. Delapalme, and J. M. Hastings, Phys. Rev. B **4**, 3206 (1971).

[11] C. G. Windsor and R. W. H. Stevenson, Proc. Phys. Soc. London **87**, 501 (1966).
[12] D. T. Teaney, M. J. Freiser, and R. W. H. Stevenson, Phys. Rev. Lett. **9**, 212 (1962).
[13] M. J. Freiser, P. E. Seiden, and D. T. Teaney, Phys. Rev. Lett. **10**, 293 (1963).
[14] M. F. Collins, *Magnetic Critical Scattering* (Oxford University Press, New York, 1989), pp. 130, 43–45.
[15] B. Fåk, M. Alba, R. Currat, and A. Brochier, ILL Report No. 91FA09T, 1991 (unpublished), p. 14.
[16] A. D. Bruce, J. Phys. C **14**, 193 (1981).
[17] A. Bunker, K. Chen, and D. P. Landau, Phys. Rev. B **54**, 9259 (1996).
[18] A. Cuccoli (private communication).
[19] M. J. Cooper and R. Nathans, Acta Crystallogr. **23**, 357 (1967).
[20] C. G. Windsor, D. H. Saunderson, and E. Schedler, Phys. Rev. Lett. **37**, 855 (1976).
[21] B. Fåk and B. Dorner, ILL Report No. 92FA008S, 1992 (unpublished).
[22] V. Privman, P. C. Hohenberg, and A. Aharony, in *Phase Transitions and Critical Phenomena*, edited by C. Domb and J. L. Lebowitz (Academic, London, 1991), Vol. 14, Chap. 1, p. 62.
[23] P. M. Horn, J. M. Hastings, and L. M. Corliss, Phys. Rev. Lett. **40**, 126 (1978).
[24] B. I. Halperin and P. C. Hohenberg, Phys. Rev. **177**, 952 (1969).